# Specific heat across the superconducting dome in the cuprates

A. J. H. Borne[1,2,3], J. P. Carbotte[4,5], and E. J. Nicol[1,2*]

[1]*Department of Physics, University of Guelph, Guelph, Ontario, Canada N1G 2W1*
[2]*Guelph-Waterloo Physics Institute, University of Guelph, Guelph, Ontario, Canada N1G 2W1*
[3]*PHELMA Grenoble INP, Minatec, 3 Parvis Louis Néel, BP 275, 38016, Grenoble, Cedex 1, France*
[4]*Department of Physics and Astronomy, McMaster University, Hamilton, Ontario, Canada L8S 4M1 and*
[5]*The Canadian Institute for Advanced Research, Toronto, Ontario, Canada M5G 1Z8*
(Dated: August 9, 2010)

The specific heat of the superconducting cuprates is calculated over the entire phase diagram. A $d$-wave BCS approach based on the large Fermi surface of Fermi liquid and band structure theory provides a good description of the overdoped region. At underdoping it is essential to include the emergence of a second energy scale, the pseudogap and its associated Gutzwiller factor, which accounts for a reduction in the coherent piece of the electronic Green's function due to increased correlations as the Mott insulating state is approached. In agreement with experiment, we find that the slope of the linear in $T$ dependence of the low temperature specific heat rapidly increases above optimum doping while it is nearly constant below optimum. Our theoretical calculations also agree with recent data on $Bi_2Sr_{2-x}La_xCuO_{6+\delta}$ for which the normal state is accessed through the application of a large magnetic field. A quantum critical point is located at a doping slightly below optimum.

PACS numbers: 74.72.-h,74.20.Mn,74..25.Bt

## I. INTRODUCTION

The superconducting state of the underdoped cuprates shows anomalous properties when compared with the case of optimum or overdoped. There has been a considerable recent effort to understand these in a model which includes the emergence of a pseudogap for doping $x$ below a quantum critical point (QCP) at $x = x_c$. The model of Yang, Rice, and Zhang[1] (YRZ) on which this work is based, has the pseudogap forming about the antiferromagnetic Brillouin zone (AFBZ) boundary with its own characteristic energy scale. This model is different in many respects from other competing order proposals such as D-density waves[2,3] and from a preformed pair model[4] which involves a single energy scale. For a review of the successes of the YRZ model in understanding the data, the reader is referred to Schachinger and Carbotte[5]. Many more details can be found in references[6–14] It is important to understand that this work goes beyond extensions of BCS theory to include effects such as strong coupling due to inelastic scattering[15–26] and possible anisotropy[27–32] beyond a simple $d$-wave superconducting gap.

In a previous work[8], we showed that the strong suppression of the specific heat jump at $T_c$ and corresponding reduction in condensation energy with increased underdoping can be understood as due to the emergence of a pseudogap. Here we consider the equally anomalous observation that the slope of the linear in temperature law as $T \to 0$ is a strongly increasing function of doping $x$ in the overdoped regime while it is nearly constant at underdoping.[33–35] While the overdoped case is characteristic of a Fermi liquid, the underdoped case requires a new ingredient for its understanding. In addition, we will also consider the recent data of Wen et al.[36] on $Bi_2Sr_{2-x}La_xCuO_{6+\delta}$ for which $T_c$ at optimum is only 30K and thus superconductivity can be quenched with a 9 Tesla magnetic field providing access to the normal state as a function of doping in both Fermi liquid (overdoped) and pseudogap (underdoped) state.

In Sec. II, we present the essential elements of the theory of YRZ[1] needed for the calculation of the specific heat. Both pseudogap state alone and with the addition of superconductivity within a BCS formulation are considered. For $x$ greater than $x_c$, the doping at which the QCP associated with the pseudogap formation is set, the Fermi surface is the usual large open contour of band theory and of a Fermi liquid. For $x < x_c$, however, the Fermi surface reconstructs into Luttinger pockets which progressively shrink in size as the Mott insulating state is more closely approached. A consequence of this is that the density of states at the Fermi level is reduced. In addition, a Gutzwiller factor enters the theory which accounts for the depletion of the coherent part of the electronic Green's function due to increased correlations which eventually cause the transition to an insulating state. In Sec. III, we present our results for the specific heat difference between superconducting and normal state as a function of temperature for values of doping ranging from 0.1 to 0.3 with $x = x_c = 0.2$ the critical doping at optimum which is also the QCP in our model. The zero temperature limit of the specific heat difference is also considered more explicitly and compared with the density of states and the data of Wen et al.[36]. In Sec. IV, we show that while pseudogap formation strongly affects the overall temperature dependence of the specific heat, it does not change its slope at low $T$. This arises because this linear law only depends on the band structure near the Dirac point on the heavily weighted part of the Fermi surface in the nodal direction and this point is not changed by pseudogap formation in the model of Ref.[1].

On the other hand the size of the slope depends directly on the Gutzwiller factor $g_t(x)$ which gives the magnitude of the remaining coherent part of the Green's function. It also depends on the ratio of the superconducting gap to critical temperature which is expected to strongly increase with decreasing doping $x$ for $x < x_c$.[5] These two effects combined lead to a rather constant value of the slope over a significant range of doping. For overdoping, Fermi liquid theory is recovered and in this case the slope shows much greater variation with $x$ as in experiment. Comparison with data is presented. In Sec. V, we provide a summary and give our conclusions.

## II. FORMALISM

In the resonating valence bond spin liquid model[1], the self-energy due to the pseudogap is given by $\Delta_{\mathrm{pg}}^2(\boldsymbol{k})/[\xi^0(\boldsymbol{k})+\omega]$, where $\xi_{\boldsymbol{k}}^0 = -2t(x)(\cos k_x a + \cos k_y a)$ with $t(x)$ the effective first neighbor hopping parameter and $\Delta_{\mathrm{pg}}(\boldsymbol{k})$ is a pseudogap which has $d$-wave symmetry in the Brillouin zone. It is given by

$$\Delta_{\mathrm{pg}}(\boldsymbol{k}) = \frac{\Delta_{\mathrm{pg}}^0(x)}{2}(\cos k_x a - \cos k_y a). \qquad (1)$$

Here the amplitude $\Delta_{\mathrm{pg}}^0(x)$ is linear in doping $x$ as shown in Fig. 1(a) where the superconducting dome is also shown for easy orientation. In the above, $\boldsymbol{k}$ is the momentum and $a$ is the lattice constant of the $CuO_2$ plane. Without superconductivity, the coherent part of the electronic Green's function is given by

$$G(\boldsymbol{k},\omega) = \frac{g_t(x)}{\omega - \xi(\boldsymbol{k}) - \Delta_{\mathrm{pg}}^2(\boldsymbol{k})/[\xi^0(\boldsymbol{k}) + \omega]}, \qquad (2)$$

where $\xi(\boldsymbol{k})$ is the electron dispersion curve of band theory and $g_t(x)$ is a Gutzwiller factor equal to $2x/(1+x)$. This latter quantity accounts for the effect of correlations which reduces the weight of the coherent part of $G(\boldsymbol{k},\omega)$ and adds an incoherent background not considered in this work. It also enters the renormalized band structure dispersion curve which includes up to third nearest neighbor hopping and narrows as the Mott transition is approached with decreasing value of $x$. This narrowing is modeled by a second Gutzwiller factor $g_s(x)$ in addition to $g_t(x)$. Effectively, for a given $\boldsymbol{k}$, there are two electron branches $E_{\boldsymbol{k}}^{\pm}$ with weights $W_{\boldsymbol{k}}^{\pm}$ given by

$$E_{\boldsymbol{k}}^{\pm} = \frac{\xi_{\boldsymbol{k}} - \xi_{\boldsymbol{k}}^0}{2} \pm \sqrt{\left(\frac{\xi_{\boldsymbol{k}} + \xi_{\boldsymbol{k}}^0}{2}\right)^2 + \Delta_{\mathrm{pg}}^2(\boldsymbol{k})} \qquad (3)$$

and

$$W_{\boldsymbol{k}}^{\pm} = \frac{1}{2}\left[1 \pm \frac{(\xi_{\boldsymbol{k}} + \xi_{\boldsymbol{k}}^0)/2}{\sqrt{[(\xi_{\boldsymbol{k}} + \xi_{\boldsymbol{k}}^0)/2]^2 + \Delta_{\mathrm{pg}}^2(\boldsymbol{k})}}\right]. \qquad (4)$$

In terms of $E_{\boldsymbol{k}}^{\pm}$, the Fermi surface contours of zero excitation energy are given by $E_{\boldsymbol{k}}^{\pm} = 0$ and these are shown in Fig. 1(b) for three values of doping $x = 0.14, 0.18$, and $0.2$. In the first two, there is a hole pocket centered about the nodal direction $\theta = \pi/4$. This pocket is determined from the equation $E_{\boldsymbol{k}}^- = 0$ and $E_{\boldsymbol{k}}^-$ is positive only for momenta falling within the area defined by the hole pocket. The size of the pocket shrinks as $x$ decreases and we come closer to half filling and the Mott insulating state. For the case $x = 0.18$, close to the QCP at $x = 0.2$ where pseudogap formation starts in our model, there is an additional electron pocket near the corner of the AFBZ. This pocket is determined by the equation $E_{\boldsymbol{k}}^+ = 0$. Both electron and hole pockets have two sides, one weighted by $W_{\boldsymbol{k}}^{\pm}$ of order one and the other, which takes on a close resemblance to the AFBZ, has only a small weight in comparison. This small weight goes to zero in the limit of no pseudogap and the energy $E_{\boldsymbol{k}}^{\pm}$ becomes the Umklapp energy surface $\xi_{\boldsymbol{k}}^0$. On the other hand, in this same limit, the heavily weighted part traces out the large Fermi surface of Fermi liquid theory (Fig. 1(b), far right panel) which has weight one everywhere. These remarks make clear the evolution from large Fermi surface into small hole pockets. As the pockets shrink in size, the number of states which carry excitations of zero energy becomes small. Also, it should be kept in mind that because of the small weight on the backside of the hole pocket, we are effectively dealing with an arc when considering many properties.

When superconductivity is included in a BCS formalism, the electronic spectral density $A(\boldsymbol{k},\omega)$ can be written in the form

$$A(\boldsymbol{k},\omega) = \sum_{\alpha=\pm} g_t(x) W_{\boldsymbol{k}}^{\alpha}[(u_{\boldsymbol{k}}^{\alpha})^2 \delta(\omega - E_{\boldsymbol{k},S}^{\alpha}) + (v_{\boldsymbol{k}}^{\alpha})^2 \delta(\omega + E_{\boldsymbol{k},S}^{\alpha})], \qquad (5)$$

with $E_{\boldsymbol{k},S}^{\alpha} = \sqrt{(E_{\boldsymbol{k}}^{\alpha})^2 + \Delta_{\mathrm{sc}}^2(\boldsymbol{k})}$. Here, the superconducting gap $\Delta_{\mathrm{sc}}(\boldsymbol{k})$ is assumed to have the same $d$-wave dependence in momentum space as in Eq. (1) for the pseudogap with amplitude $\Delta_{\mathrm{sc}}^0(x)$ replacing $\Delta_{\mathrm{pg}}^0(x)$ and $\Delta_{\mathrm{sc}}^0(x)$ is assumed to have the same doping dependence as the critical temperature $T_c(x)$ dome. This is shown in Fig. 1(a) and for definiteness we will assume in all our numerical work that $2\Delta_{\mathrm{sc}}^0(x)/k_B T_c(x) = 6$. When later we compare with experimental data, we will remove this simplifying assumption. The Bogoliubov weights in Eq. (5) are

$$(u_{\boldsymbol{k}}^{\alpha})^2 = \frac{1}{2}\left(1 + \frac{E_{\boldsymbol{k}}^{\alpha}}{E_S^{\alpha}}\right), \qquad (6)$$

$$(v_{\boldsymbol{k}}^{\alpha})^2 = \frac{1}{2}\left(1 - \frac{E_{\boldsymbol{k}}^{\alpha}}{E_S^{\alpha}}\right). \qquad (7)$$

The dispersion curves for $\xi_{\boldsymbol{k}}$ and $\xi_{\boldsymbol{k}}^0$ are taken from the work of Ref.[1] and are unchanged here as are the other parameters, namely,

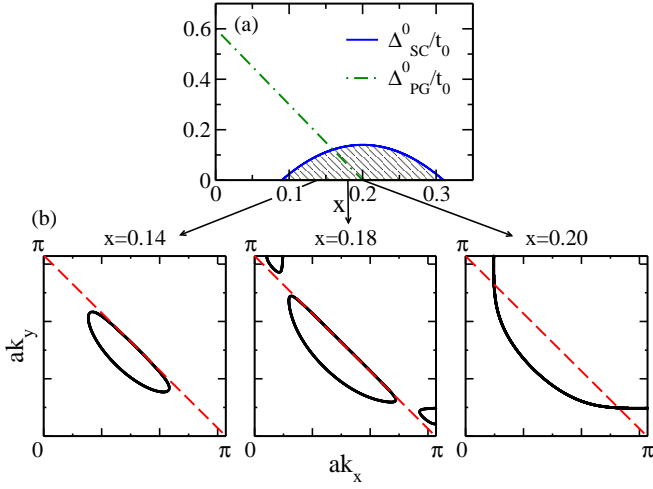$$\Delta_{\mathrm{sc}}^0(x) = 0.14 t_0[1 - 82.6(x - 0.2)^2] \qquad (8)$$

FIG. 1: (Color online) (a) Phase diagram for the model discussed in the paper, showing the pseudogap $\Delta^0_{pg}$ and superconducting gap $\Delta^0_{sc}$ in units of $t_0$ as a function of doping $x$. (b) Illustration of the reconstruction of the Fermi surface in the first quadrant of the Brillouin zone for doping values of $x = 0.14$, $0.18$ and $0.2$. The red dashed line is the AFBZ boundary.

and

$$\Delta^0_{pg}(x) = 3t_0(0.2 - x), \qquad (9)$$

with $t_0$ an unrenormalized nearest neighbor hopping parameter characteristic of the CuO$_2$ plane.

There are two equivalent ways for calculating the specific heat $C_V(T) \equiv \gamma(T)T$. One is through the entropy $S(T)$, the other through the internal energy $U(T)$. The entropy is

$$S(T) = -2k_B g_t(x) \sum_{\boldsymbol{k},\alpha=\pm} W^{\alpha}_{\boldsymbol{k}} \{ f(E^{\alpha}_{\boldsymbol{k}S}) \ln f(E^{\alpha}_{\boldsymbol{k}S})$$
$$+ [1 - f(E^{\alpha}_{\boldsymbol{k}S})] \ln[1 - f(E^{\alpha}_{\boldsymbol{k}S})] \}, \qquad (10)$$

where $f(x)$ is the Fermi-Dirac temperature distribution function. Alternatively, the internal energy can be expressed in terms of the single spin density of states $N(\omega)$ as

$$U(T) = 2 \int_{-\infty}^{\infty} \omega N(\omega) f(\omega) d\omega \qquad (11)$$

where the two is for spin degeneracy and the density of states is given by

$$N(\omega) = \sum_{\boldsymbol{k},\alpha=\pm} g_t(x) W^{\alpha}_{\boldsymbol{k}} [(u^{\alpha}_{\boldsymbol{k}})^2 \delta(\omega - E^{\alpha}_{\boldsymbol{k},S}) + (v^{\alpha}_{\boldsymbol{k}})^2 \delta(\omega + E^{\alpha}_{\boldsymbol{k},S})].$$
$$(12)$$

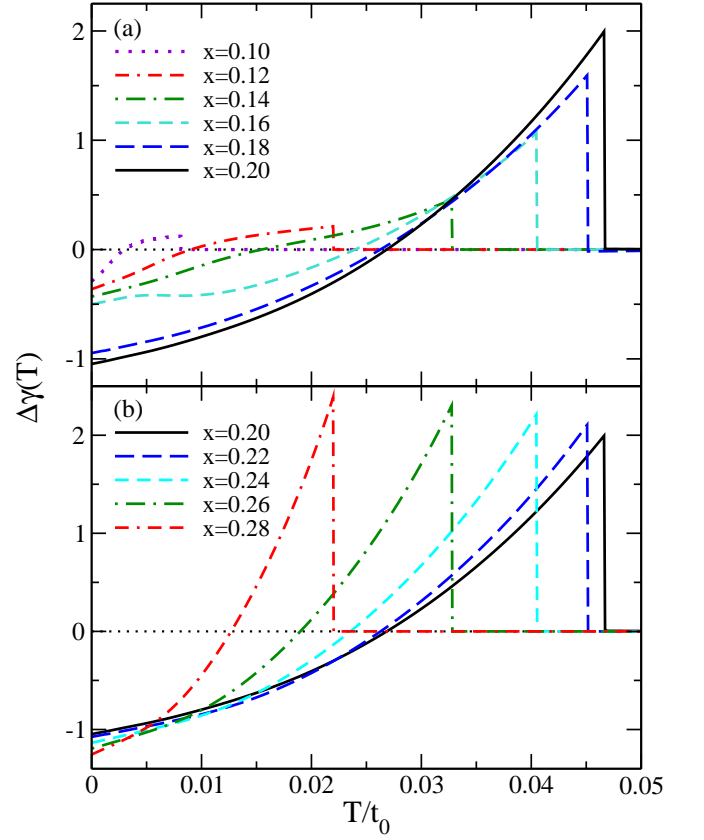In both Eqs. (10) and (12), the sum is over the entire Brillouin zone and $C_V(T) = dU(T)/dT = \gamma(T)T$.



FIG. 2: (Color online) $\Delta\gamma(T)$ versus $T/t_0$, where $\Delta\gamma \equiv \gamma_{sc} - \gamma_n$ is in units of $k_B^2/t_0$ per volume. Curves are shown for (a) underdoped and (b) overdoped cases along with optimal doping for reference.

## III. NUMERICAL RESULTS FOR THE SPECIFIC HEAT

In Fig. 2, we present our results for the difference between the superconducting and normal state specific heat $\gamma(T)$, namely $\Delta\gamma(x, T) \equiv \gamma_{sc}(x, T) - \gamma_n(x, T)$ in units of $k_B^2/t_0$ per volume as a function of temperature $T$. Several values of doping $x$ are considered as indicated in the figure. The top frame covers the underdoped regime, while the bottom frame is for overdoped. As the superconducting dome given in Eq. (8) is symmetric in doping about optimum $x = 0.2$, the top and bottom frame curves come in pairs with the same value of critical temperature (with the exception of not displaying $x = 0.3$ for clarity). Comparison of top and bottom curves in a given pair shows that the formation of a pseudogap and associated Fermi surface reconstruction [Fig. 1(b)] provides a drastic suppression of the jump at the critical temperature $T_c$ and also of the slope just below $T_c$. This is in qualitative agreement with experiment[33–36], as discussed already in Ref.[8]. These results are clearly not part of ordinary $d$-wave BCS theory where instead the jump is large and relatively independent of doping as seen in the Fig. 2(b). For reference in assessing these curves, we recall that for
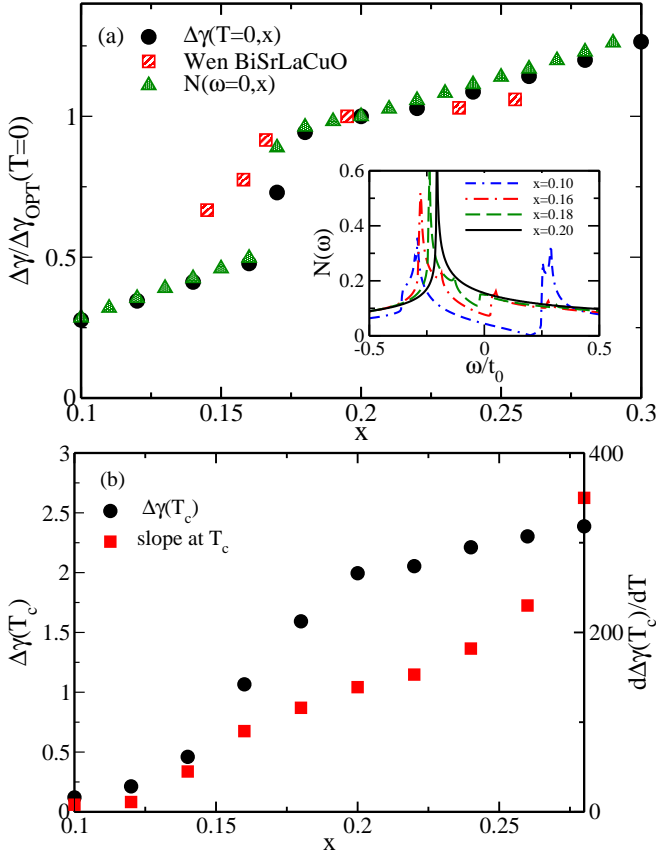
FIG. 3: (Color online) (a) $\Delta\gamma$ as $T \to 0$ normalized to the same quantity at optimal doping versus doping $x$. Values extracted from the data of Wen et al.[36] are shown along with the DOS at zero energy $N(0)$ similarly normalized. The inset shows $N(\omega)$ in units of $t_0$ for several dopings as a function of $\omega/t_0$. $N(\omega)$ and $N(0)$ refer to the normal state with a pseudogap. (b) Value of $\Delta\gamma$ at $T_c$ from Fig. 2 (left axis) and slope just below $T_c$, $d\Delta\gamma(T_c)/dT$ (right axis) as a function of $x$.

a constant density of states model with a superconducting $d$-wave gap defined on the Fermi surface, the canonical value of the jump $\Delta\gamma(T_c)/\gamma_n(T_c)$ is 0.95 for a gap to critical ratio $2\Delta_{sc}^0/k_B T_c = 4.3$ and is the same for all superconductors regardless of the size of $T_c$. Here it deviates from this universal law because our superconducting gap is defined in the entire Brillouin zone according to Eq. (1) with the pseudogap replaced by $\Delta_{sc}^0$ and our energy bands can be complicated even when the large Fermi surface of Fermi liquid theory is involved. Also, the magnitude of the jump itself is increased because we have used a gap to $T_c$ ratio of 6 rather than the weak coupling limit of 4.3 and this has resulted in a change of $\Delta\gamma(T_c)/\gamma_n(T_c)$ from 0.95 to $\sim 1.7$. Thus, the large decrease in the jump $\Delta\gamma(T_c)$ seen in Fig. 2(a) is a direct consequence of pseudogap formation and accompanying Fermi surface reconstruction.

The size of the specific heat difference seen at zero temperature is also of interest and is very different in

the underdoped than in the overdoped regime. While for near optimum, optimum and overdoped cases the value of $\Delta\gamma(T)$ as $T \to 0$ is around -1 in our units, for the underdoped cases, it has moved instead to a value of roughly $\sim -0.5$. In this limit $\Delta\gamma(T = 0)$ simply reduces to its normal state value $\gamma_n$ and is a direct measure of the value of the density of states $N(\omega)$ at the Fermi energy, *i.e.* at $\omega = 0$. In Fig. 3(a), we compare the results of our calculations for $\Delta\gamma(T = 0)/\Delta\gamma_{OPT}(T = 0)$ (circles) with the specific heat data of Wen et al.[36] on $Bi_2Sr_{2-x}La_xCuO_{6+\delta}$ (squares). Here, OPT refers to the value taken at optimal doping ($x = 0.2$ in our model). In carrying out this comparison, we have fit a parabolic form to the data of Wen et al. for $T_c$ versus doping. We found that the fit which best captured the data was when optimum was taken at their doping of $p = 0.165$ and $t_0$ is set to 56 meV for $2\Delta_0/k_B T_c = 6$. Similar, but less ideal fits would also work for optimum at $p = 0.16$. Note that this material does not have a very high $T_c$ and consequently has a narrower dome compared with what is typically found in the literature. It was chosen for experiment because reasonable magnetic fields can be used to suppress $T_c$ to zero and so access the normal state. Given our fit, we have shifted the value of $p$ in experiment by 0.035 to get correspondence with our theoretical work for which $x$ at optimum is kept at $x = 0.2$. Further discussion of this is presented in Sec. IV. We have kept the pseudogap line to be as shown in Fig. 1(a) which coincides with optimum doping, but this could easily be changed. Returning to Fig. 3(a), both theory and experiment show two distinct regimes: a somewhat flat or slowly rising region above $x \simeq 0.17$ with a sharp drop below this value. The behavior in the region above $x = 0.2$ is sensitive to the choice of bandstructure parameters as shown in the original work of YRZ (Ref.[1]). Because the data is fairly flat in this region, we have opted to alter the bandstructure accordingly and have allowed the $t'$ and $t''$ parameters to continue to vary with $x$ rather than to become constant for $x > 0.2$ as in Ref.[1]. Returning to the rapid drop around $x \sim 0.17$, we find that it is displaced to slightly lower values of $x$ in the data as compared to theory and we take this to mean that in $Bi_2Sr_{2-x}La_xCuO_{6+\delta}$ the QCP associated with the start of pseudogap formation occurs at a doping level close but slightly below optimum. It is important to realize that in the present model, the point at which the value of the density of states at the Fermi level $N(0)$ begins to be strongly reduced by the growth of the pseudogap, is not exactly at the QCP but is instead displaced to smaller $x$ values. The physics of this displacement is easily understood with reference to the inset in Fig. 3(a). First we show, in the main frame, that our numerical results for $N(0)$ versus $x$ (triangles) are very close to the solid black circles as they must be. These were obtained not from an extrapolation to zero temperature of a specific heat calculation as were the solid circles but instead from the full DOS $N(\omega)$ versus $\omega$ shown in the inset. This good agreement is taken as providing a check on our numerical work. More signif-

icantly it is important to realize that the Fermi surface reconstruction from the large open Fermi liquid surface of Fig. 1 ($x = 0.2$) to a Luttinger hole pocket does not immediately lead to change in the value of $N(0)$. In fact, as can be seen clearly in the inset of Fig. 3(a), at $x = 0.18$ the DOS at $\omega = 0$ is hardly changed from its Fermi liquid value (see solid black curve for $x = 0.2$ for comparison). Rather the effect of the pseudogap is to provide a depletion of states at negative $\omega$. For $x = 0.16$ however, the upper edge of this depletion region which is rather sharp, has moved across the Fermi energy and $N(0)$ has become significantly reduced as shown in the triangles of the main frame in Fig. 3(a). This is not surprising. The DOS at $\omega = 0$ depends on the Luttinger contours of zero energy shown in Fig. 1. At $x = 0.18$, there are both hole and electron pockets and the number of states having zero energy is not very different from the number when the large open Fermi surface applies. It is only when we reach a single small hole pocket and no electron pockets that depletion of states at $\omega = 0$ becomes significant. On the face of it, one might even think that more zero energy states are involved when $x = 0.18$ than when $x = 0.2$ because the length of the Fermi surface is larger when there are pockets. But this is not so because, as we have already stated, parts of the Luttinger contours carry very little weight.

In Fig. 3(b), we show results for the jump at $T_c$ of the specific heat $\Delta\gamma(T_c)$ (circles) and its slope out of $T_c$ (squares) as a function of doping. We note that for the jump $\Delta\gamma(T_c)$, a notable drop occurs almost immediately below optimum $x = 0.2$, which can be used to identify the QCP. For the slope, the signature of the QCP is not as sharp, only a change in curvature arises at $x = 0.2$. These results are to be contrasted with those in Fig. 3(a). If one were to estimate the value of doping to be associated with the QCP from the behavior of $\Delta\gamma(T)$ at $T \to 0$, it is necessary to account for a significant displacement downward towards smaller values of $x$ of the rapid drop in $N(0)$ as compared to the value of $x$ at the QCP. Thus extracting a QCP from thermodynamics requires some care but it clearly can be done either from the jump at $T_c$ or the value of the difference $\Delta\gamma(T)$ as $T \to 0$.

## IV. LOW TEMPERATURE BEHAVIOR

We now consider the low temperature behavior of the superconducting state specific heat $\gamma_{sc}(T)$ which is emphasized in Fig. 4(a)-(d) for underdoped cases. We base our discussion on the physics of the schematic shown in Fig. 4(e). The Luttinger pockets are shown as heavy black lines for $x = 0.18$ which has electron as well as hole areas. Also shown is a Dirac cone centered on the highly weighted Fermi surface contour in the nodal direction. The cone illustrates the quasiparticle energies at low energy in the superconducting state as a function of $k_x$ and $k_y$ in the Brillouin zone. Only the upper right quadrant is depicted. At very low temperatures, the tip of this cone is the only region in momentum space where there is a finite thermal occupation of excited quasiparticles. Thus, the specific heat can depend only on characteristic parameters associated with the Dirac point. But this point is particularly simple. It corresponds to $E_{\boldsymbol{k}}^- = 0$ in the normal pseudogap case and does not change with the onset of superconductivity. In the nodal direction, the pseudogap $\Delta_{\mathrm{pg}}(\boldsymbol{k}) = 0$ and therefore $\xi_{\boldsymbol{k}} = 0$ which is the condition for the underlying large Fermi surface. Note that strictly speaking $\xi_{\boldsymbol{k}}$ involves the chemical potential $\mu_p$ associated with the case when the pseudogap is present and is slightly different from the chemical potential of Fermi liquid theory. In the former case, it is determined from the Luttinger sum rule while in the latter case of a large Fermi surface one might determine $\mu_p$ from the DOS filling up to $\boldsymbol{k} = \boldsymbol{k}_F$. Neglecting this small difference, the band energy at the Dirac point is unchanged from its Fermi liquid value and the well known techniques[37] for obtaining the $\omega \to 0$ limit of the DOS $N(\omega)$ apply unaltered. The result is

$$N(\omega) \simeq |\omega| \frac{g_t(x)}{\pi v_F v_\Delta}, \qquad (13)$$

where $v_F$ and $v_\Delta$ are the Fermi and gap velocity, respectively. Note that Eq. (13) predicts that the only effect of the pseudogap formation on the DOS around the Dirac point is the appearance of the Gutzwiller factor $g_t(x)$. While to a good approximation $v_F$ is unchanged, the gap velocity can be changed in magnitude if the ratio of zero temperature gap to critical temperature $T_c$ is affected by pseudogap formation as was found in the recent work of Schachinger and Carbotte[5]. This provides a second important change in Eq. (13) as compared with the more familiar Fermi liquid case.

Inserting Eq. (13) into Eq. (11) for the internal energy $U(T)$, we obtain the simple analytic result for $\gamma_{sc}(T)$ in the limit of low temperature:

$$\gamma_{sc}(T) = 4k_B^2(k_B T) \frac{g_t(x)}{\pi v_F v_\Delta} h, \qquad (14)$$

where $k_B$ is the Boltzmann constant and $h$ is a number given by

$$h = 4 \int_{-\infty}^{+\infty} dy |y|^3 \cosh^{-2}(y) \simeq 5.4. \qquad (15)$$

We have obtained, as in ordinary $d$-wave BCS theory, a linear in $T$ law with the same material factors appearing, i.e. $v_F$ and $v_\Delta$, but with an extra Gutzwiller factor of $g_t(x)$. We also need to note that $\Delta$ can be affected by the variation with doping $x$ of the gap ratio $R(x) \equiv 2\Delta_{\mathrm{sc}}^0(x)/k_B T_c(x)$.

In Fig. 4, we show our numerical results for $\gamma_{sc}(T)$ at four values of $x$ namely 0.12, 0.14, 0.16 and 0.18. In all cases, the solid line is for the case when no pseudogap is included while the dashed-dotted includes a pseudogap with its magnitude chosen to correspond to the value of
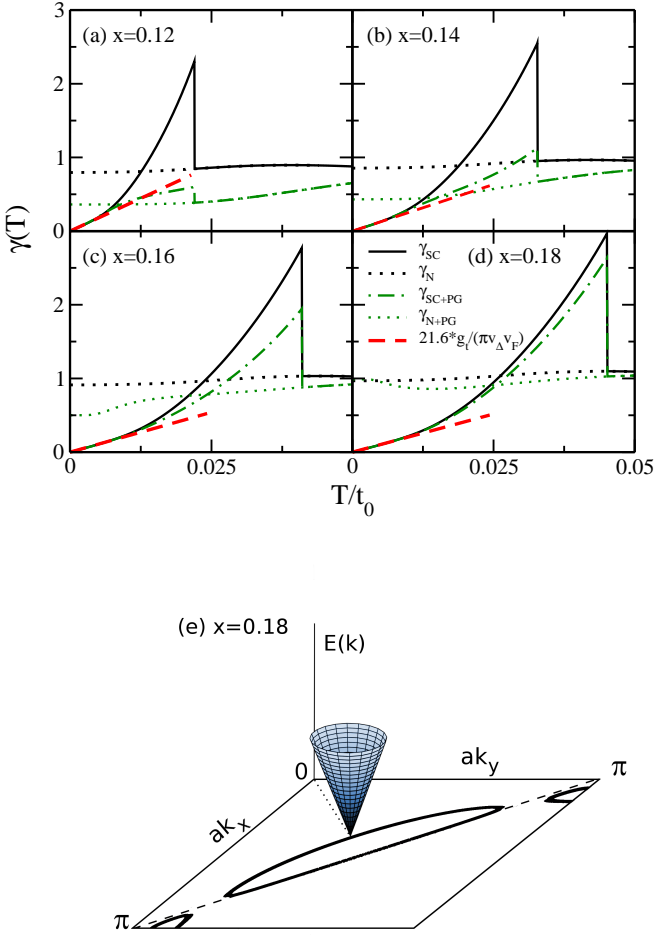
FIG. 4: (Color online) $\gamma(T)$ versus $T/t_0$ shown in the absence of any gaps $\gamma_N$, with superconductivity only $\gamma_{SC}$, pseudogap only $\gamma_{PG}$ and with both gaps present $\gamma_{SC+PG}$. The red dashed line gives the theoretical expression for the slope from Eq. (14). (a)-(d) show a range of dopings for the underdoped case. (e) Schematic of the superconducting Dirac cone shown on the side of the $x = 0.18$ Fermi pocket with large quasiparticle weight.

doping $x$ chosen. Otherwise, there are no other changes. Gutzwiller factors are included in these curves and the ratio $R(x)$ is fixed at value 6 as in all other numerical work presented in this paper. While the inclusion of a pseudogap has drastic effects on $\gamma_{sc}(T)$, the slope as $T \to 0$ is completely unaffected and this slope agrees perfectly with the simplified analytic results of Eq. (14) given as the red dashed line. This constitutes an important prediction of YRZ theory and will be verified later when we make comparison with experimental data.

The heavy dotted lines in Fig. 4 show the normal state specific heat $\gamma_N(T)$ in the Fermi liquid and the light dotted, with a pseudogap included $\gamma_{N+PG}(T)$. It is instructive to consider these in some detail and in particular to describe how they are related to the detailed variation of $N(\omega)$ versus $\omega$ in the pure pseudogap state, i.e. with no superconductivity. We begin with the case $x = 0.18$

for which the pseudogap is small and the Fermi contours include electron as well as hole pockets. In this case, the light dotted curve falls below the heavy dotted one but rises to meet it as $T \to 0$. This behavior can be traced to the $\omega$ variation seen in the inset of Fig. 3(a) which shows $N(\omega)$ versus $\omega$. The solid black curve forms a reference and is the Fermi liquid result for $x = 0.2$, zero pseudogap. Comparing with the long-dashed green curve for $x = 0.18$, we note no visible change in the value of $N(\omega = 0)$ but there is a significant depression of DOS at negative energies. As $T \to 0$ only $N(0)$ is sampled in the specific heat and hence both cases, with and without a pseudogap, agree. At small but finite $T$, however, the light-dotted curve falls below the heavy dotted line in Fig. 4(d) because the dip in its DOS at $\omega < 0$ starts to be sampled and this reduces the specific heat. Specific heat is, however, a rather broad spectroscopy for $N(\omega)$ because the thermal factor in $\gamma(T)$ in Eq. (11) samples of order $5k_BT$ or so about $\omega = 0$. The case $x = 0.12$ is also noteworthy. In this instance the DOS about the Fermi energy is nearly monotonic although depressed in value as compared to $x = 0.2$ by about 50% and this correspondingly reduces the value of $\gamma_N(T)$ by the same amount with little other changes.

We turn next to a comparison with data on the slope of the specific heat in the $T \to 0$ limit. These are presented in Fig. 5(a) for the $Bi_2Sr_{2-x}La_xCuO_{6+\delta}$ data of Wen et al.[36] and in (b) for the data on Bi-2212 and (Y,Ca)-123 of Loram et al.[33–35] where we have read slopes from the published figures as best as was possible. A more thorough analysis by the experimentalists might achieve better accuracy. In the inset of Fig. 5(a), we show our results for the fit to the $T_c$ dome of the Wen et al.[36] data. We find

$$k_BT_c = \frac{0.14}{3}[1 - 225(p - 0.165)^2]t_0, \qquad (16)$$

which provides a good representation of the $T_c$ data as a function of doping $p$. We then take $x = p + 0.035$ to place the data on our curves. In the main frame, the solid black circles are the data for the slope at $T \to 0$ normalized to its value at optimum doping. The solid red line gives results of Eq. (14) with the assumption of $R = 6$. The agreement is very good and the sharp rise in slope in the overdoped region is captured by our model. For the deeply underdoped case, our theoretical values are somewhat higher than experiment, but as we have already mentioned, the gap ratio may well vary with doping. Solving a BCS-like pairing equation with pseudogap formation and corresponding Fermi surface reconstruction accounted for, Schachinger and Carbotte[5] found that (for $x \leq 0.2$) approximately

$$R(x) \sim 4.3[1 + 75(x - 0.2)^2]. \qquad (17)$$

If this correction, scaled to 6 at optimum, is incorporated into the comparison with experiment, we get the red dashed curve which agrees better with the data at small $x$. Note finally that to compare data with theory,
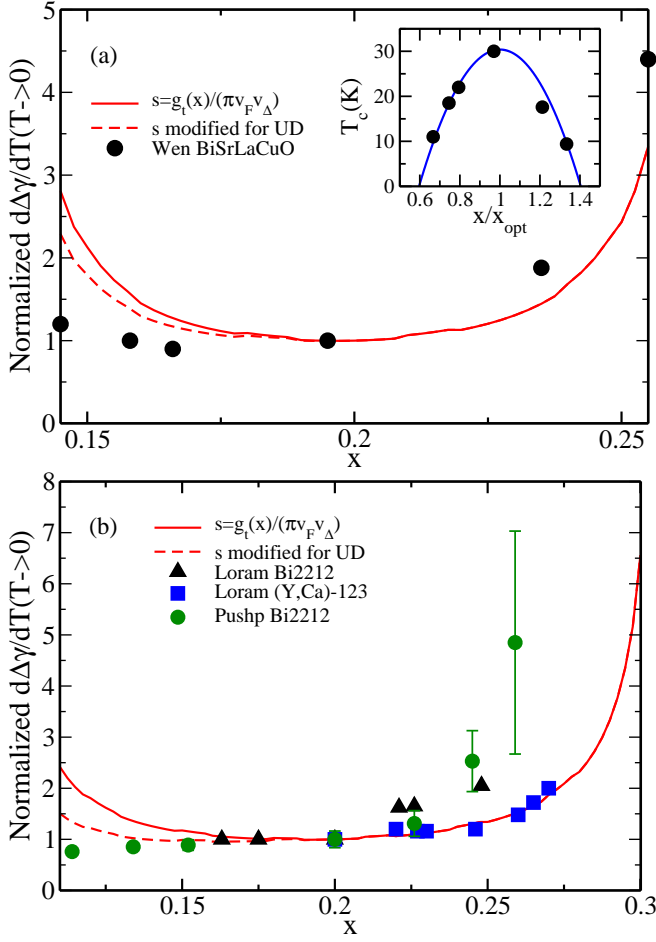
FIG. 5: (Color online) The slope of the specific heat at low $T$ normalized to the value at optimal doping. Frame (a) shows the data extracted from Wen et al.[36] compared with the theory of Eq. (14) for the $T_c$ dome given in the inset where we have fit a functional form for $x$ to their $T_c$ data (see text for discussion). The dashed curve includes the correction $R(x)$ discussed in the text. (b) The extracted data of Loram et al.[33–35] is compared to the theoretical slope. Shown also is the slope data from the STS DOS of Pushp et al.[38].

we have shifted all $x$ values in Fig. 5(a) by 0.035 because we wished to remain, as in the paper of YRZ[1], with optimum doping at $x = 0.2$ rather than the experimental value of about 0.165. This is also true for Fig. 5(b) where we compare with data on Bi2212 (triangles) and (Y,Ca)-123 (squares). The agreement with theory (solid and dashed red curves) is again good. We have also included one further comparison with scanning tunneling spectroscopy (STS) results on Bi2212 by Pushp et al.[38] (circles). STS gives the DOS and not the specific heat, but this latter quantity follows directly from a knowledge of $N(\omega)$. We can use the STS data in the limit of $\omega \to 0$ to determine $N(\omega)$ as in Eq. (13) and so get $\gamma_{sc}(T)$ for $T \to 0$. These are the solid circles which provide a confirmation of the specific heat results and also provide a significant cross check between these two important but very different probes of the microscopic structure of the superconducting state in the underdoped cuprates and indeed over the entire phase diagram.

## V. SUMMARY AND CONCLUSIONS

The behavior of the specific heat of the underdoped cuprates differs profoundly from that observed on the overdoped side of their phase diagram. At optimum and overdoping, an ordinary BCS approach based on a Fermi liquid normal state with constant DOS provides a first reasonable understanding on the assumption that the gap has $d$-wave symmetry. This ensures a linear in $T$ low temperature law for the specific heat $\gamma(T)$ with $C_V(T) = \gamma(T)T$. It also gives a jump at $T_c$ normalized to its normal state value of 0.95 and this value can be increased if the gap to $T_c$ ratio is changed from 4.3 to a higher value. On the deeply underdoped side, however, there is new physics which cannot be described even when strong coupling effects[15–26] due to inelastic scattering[19–26] are accounted for and/or effects of anisotropy[27–32]. which go beyond a simple lowest harmonic $d$-wave picture for the superconducting gap.

In the resonating valence bond spin liquid picture, a second energy scale, the pseudogap, emerges and grows in magnitude as $x$ is reduced towards the Mott insulating state. This pseudogap leads to a loss of metallicity. It also radically reduces the size of the specific heat jump at $T_c$ as noted in experiment[33–35] and also in theory[8]. However, as we show here the limit of $T \to 0$ of $\gamma_{sc}(T)$ is not directly affected by the size of $\Delta_{pg}^0$ because this limiting value depends only on the band structure and superconducting gap right at the Dirac point in the Brillouin zone. But this point is not importantly changed by pseudogap formation and Fermi surface reconstruction so that the formula for the slope $d\gamma_{sc}(T)/dT$ as $T \to 0$ remains unchanged in form but with two important modifications. First, in the resonating valence bond spin liquid, there appears a Gutzwiller factor $g_t(x)$ which depends strongly on doping $x$ and represents the remaining weight in the coherent part of the electronic Green's function as correlations become more important and consequently shift more spectral weight into an incoherent background at higher energies. A second factor is that the ratio of $2\Delta_{sc}^0(x)/k_B T_c(x) = R(x)$ can vary with doping. For overdoped and optimally doped, in ordinary BCS $d$-wave it has a value of 4.3, but Schachinger and Carbotte[5] have found that it rises considerably in the underdoped region of the phase diagram. These authors solve a BCS gap equation generalized to include pseudogap formation and attendant Fermi surface reconstruction. The results of such a theoretical study show that $R(x)$ increases beyond a value of 7 before the lower end of the superconducting dome is reached. These two effects, along with the linear in $T$ law which we have shown to still hold in YRZ theory at underdoping, allow us to understand a previously anomalous feature of

the data namely the slope remains reasonably constant at underdoping while it increases sharply in the overdoped region. This last observation is consistent with a slope which varies inversely as the gap and this gap decreases toward zero as we approach the upper end of the dome. Comparison between theory and data on BiSrLaCuO, Bi2212, and (Y,Ca)-123 show good agreement. A further comparison was made with STS data which provides information on the average density of quasiparticle states. It was noticed by Pushp et al.[38] that the slope of this quantity, in the $\omega \to 0$ limit, while increasing with reduced value of $T_c$ at overdoping, saturates and perhaps even decreases slightly with decreasing $x$ in the highly underdoped regime. But the low $\omega$ dependence of the DOS determines the low temperature behavior of the specific heat. For the specific case of Bi2212, we found good agreement between STS and specific heat data further confirming our work and providing a strong test of the consistency between experimental data obtained by these two very different techniques and their consistency with the resonating valence bond spin liquid.

\* Electronic address: enicol@uoguelph.ca

[1] K.-Y. Yang, T. M. Rice and F. C. Zhang Phys. Rev. B **73**, 174501 (2006).

[2] S. Chakravarty, R. B. Laughlin, D. K. Morr, and C. Nayak, Phys. Rev. B **63**, 094503 (2001).

[3] J.-X. Zhu, W. Kim, C. S. Ting, and J. P. Carbotte, Phys. Rev. Lett. **87**, 197001 (2001).

[4] V. J. Emery and S. A. Kivelson, Nature (London) **374**, 434 (1995).

[5] E. Schachinger and J. P. Carbotte, Phys. Rev. B **81**, 014519 (2010).

[6] B. Valenzuela and E. Bascones, Phys. Rev. Lett. **98**, 227002 (2007).

[7] J. P. F. LeBlanc, J. P. Carbotte, and E. J. Nicol, Phys. Rev. B **81**, 064504 (2010).

[8] J. P. F. LeBlanc, E. J. Nicol, and J. P. Carbotte, Phys. Rev. B **80**, 060505(R) (2009).

[9] J. P. Carbotte, K. A. G. Fisher, J. P. F. LeBlanc, and E. J. Nicol, Phys. Rev. B **81**, 014522 (2010).

[10] E. Illes, E. J. Nicol, and J. P. Carbotte, Phys. Rev. B **79**, 100505(R) (2009).

[11] E. Bascones and B. Valenzuela, Phys. Rev. B **77**, 024527 (2008).

[12] K.-Y. Yang, H. B. Yang, P. D. Johnson, T. M. Rice and F. C. Zhang, EPL **86**, 37002 (2009).

[13] K.-Y. Yang, K. Huang, W.-Q. Chen, T. M. Rice and F. C. Zhang, arXiv:1005.3441

[14] A. J. H. Borne, J. P. Carbotte, and E. J. Nicol, Phys. Rev. B **82**, 024521 (2010).

[15] B. Mitrovic, C. R. Leavens, and J. P. Carbotte, Phys. Rev. B **21**, 5048 (1980).

[16] E. Schachinger, J. M. Daams, and J. P. Carbotte, Phys. Rev. B **22**, 3194 (1980).

[17] H. K. Leung, J. P. Carbotte, D. W. Taylor, and C. R. Leavens, Can. J. Phys. **54**, 1585 (1976).

[18] F. Marsiglio, R. Akis, and J. P. Carbotte, Phys. Rev. B **36**, 5245 (1987).

[19] J. P. Carbotte, E. Schachinger, and J. Hwang, Phys. Rev. B **71**, 054506 (2005).

[20] E. Schachinger, J. J. Tu, and J. P. Carbotte, Phys. Rev. B **67**, 214508 (2003).

[21] J. P. Carbotte, C. Jiang, D. N. Basov, and T. Timusk, Phys. Rev. B **51**, 11798 (1995).

[22] E. J. Nicol, J. P. Carbotte, and T. Timusk, Phys. Rev. B **43**, 473 (1991).

[23] F. Marsiglio, J. P. Carbotte, A. Puchkov, and T. Timusk, Phys. Rev. B **53**, 9433 (1996).

[24] E. J. Nicol and J. P. Carbotte, Phys. Rev. B **44**, 7741 (1991).

[25] E. Schachinger, J. P. Carbotte, and F. Marsiglio, Phys. Rev. B **56**, 2738 (1997).

[26] E. Schachinger and J. P. Carbotte, Phys. Rev. B **62**, 9054 (2000).

[27] P. G. Tomlinson and J. P. Carbotte, Phys. Rev. B **13**, 4738 (1976).

[28] H. K. Leung, J. P. Carbotte, and C. R. Leavens, J. Low Temp. Phys. **24**, 25 (1976).

[29] C. O'Donovan and J. P. Carbotte, Phys. Rev. B **52**, 4568 (1995).

[30] C. O'Donovan and J. P. Carbotte, Physica C **252**, 87 (1996).

[31] D. Branch and J. P. Carbotte, Phys. Rev. B **52**, 603 (1995).

[32] C. O'Donovan and J. P. Carbotte, Phys. Rev. B **52**, 16208 (1995).

[33] J. W. Loram, J. L. Tallon, and W. Y. Liang, Phys. Rev. B **69**, 060502(R) (2004).

[34] J. W. Loram, K. A. Mirza, J. R. Cooper, and J. L. Tallon, Physica C **282-287**, 1405 (1997).

[35] J. G. Storey, J. L. Tallon, G. V. M. Williams, and J. W. Loram, Phys. Rev. B **76**, 060502(R) (2007).

[36] H.-H. Wen, et al., Phys. Rev. Lett. **103**, 067002 (2009).

[37] A. C. Durst and P. A. Lee, Phys. Rev. B **62**, 1270 (2000).

[38] A. Pushp, C. V. Parker, A. N. Pasupathy, K. K. Gomes, S. Ono, J. Wen, Z. Xu, G. Gu, and A. Yazdani, Science **324**, 1689 (2009).